

Chemical Science

Accepted Manuscript



This article can be cited before page numbers have been issued, to do this please use: M. Briganti, G. Fernandez Garcia, J. Jung, R. Sessoli, B. Le Guennic and F. Totti, *Chem. Sci.*, 2019, DOI: 10.1039/C9SC01743G.



This is an Accepted Manuscript, which has been through the Royal Society of Chemistry peer review process and has been accepted for publication.

Accepted Manuscripts are published online shortly after acceptance, before technical editing, formatting and proof reading. Using this free service, authors can make their results available to the community, in citable form, before we publish the edited article. We will replace this Accepted Manuscript with the edited and formatted Advance Article as soon as it is available.

You can find more information about Accepted Manuscripts in the [author guidelines](#).

Please note that technical editing may introduce minor changes to the text and/or graphics, which may alter content. The journal's standard [Terms & Conditions](#) and the ethical guidelines, outlined in our [author and reviewer resource centre](#), still apply. In no event shall the Royal Society of Chemistry be held responsible for any errors or omissions in this Accepted Manuscript or any consequences arising from the use of any information it contains.

ARTICLE

Covalency and magnetic anisotropy in Lanthanide Single Molecule Magnets: the DyDOTA Archetype

Matteo Briganti,^a Guglielmo Fernandez Garcia,^{ab} Julie Jung,^{b†} Roberta Sessoli,^a Boris Le Guennic,^{*b} and Federico Totti^{*a}Received 00th January 20xx,
Accepted 00th January 20xx

DOI: 10.1039/x0xx00000x

Lanthanide ions when complexed by polyamino-polycarboxylate chelators form a class of compounds of paramount importance in several research and technological areas, as, for instance, in the fields of magnetic resonance and molecular magnetism. Indeed, the gadolinium derivative is one of the most employed contrast agents for magnetic resonance imaging while the dysprosium one belongs to the new generation of contrast agents for T₂-weighted MRI. In molecular magnetism, Single Molecule Magnets (SMMs) containing lanthanide ions have become readily popular in the chemists and physics communities since record energy barriers to the reversal of magnetization were reported. The success of lanthanide complexes resides in their large anisotropy due to the contribution of the unquenched orbital angular momentum. However, only few efforts have been done so far to understand how the f-orbitals can be influenced by the surrounding ligands. The outcomes have been rationalized by mere electrostatic perturbation models. In the archetype compound [Na{Dy(DOTA)(H₂O)}]·4H₂O (DyDOTA) an unexpected easy axis of magnetization perpendicular to the pseudo-tetragonal axis of the molecule was found. Interestingly, a dependency of the orientation of the principal magnetization axis by the simple rotation of the coordinating apical water molecule (AWM) - highly relevant for MRI contrast - around the Dy-O_{AWM} bond was predicted by *ab initio* calculations, too. However, such a behaviour has been contested in a following paper justifying their conclusions on pure electrostatic assumptions. In this paper, we want to shed some light on the nature of the subtle effects induced by the water molecule on the magnetic properties of the DyDOTA archetype complex. Therefore, we have critically reviewed the structural models already published in literature along with new ones showing how the easy axis orientation can dangerously depend on the chosen model. The computed different behavior of the orientation of the easy axis of magnetization has been rationalized as a function of the energy gap between the ground and the first excited doublet. Magneto-structural correlations together with a mapping of the electrostatic potential generated by the ligands around the Dy(III) ion through a multipolar expansion have also evidenced and quantified the covalent contribution of the AWM orbitals.

Introduction

Lanthanide ions when complexed by polyamino-polycarboxylate chelators form a class of compounds of paramount importance in several research and technological areas, particularly in the fields of magnetic resonance¹ and molecular magnetism^{2–4}. One of the paradigmatic ligand of this class of complexes is the twelve-membered tetraazamacrocyclic H₄DOTA (1,4,7,10-tetraazacyclododecane-1,4,7,10-N,N',N'',N'''-tetraacetic acid). In its fully deprotonated form, DOTA⁴⁻, it yields thermodynamically and kinetically stable compounds⁵ with the whole series of trivalent lanthanide ions Ln³⁺ giving a capped square antiprismatic coordination

geometry (coordination number 9). The rare earth ion is sandwiched between two parallel square faces, one formed by the ligand's four nitrogen atoms and the other by four oxygen atoms of the four acetate groups. The ninth coordination site along the pseudo C₄ axis is occupied by a non-innocent apical water molecule (AWM) which contributes to the unique properties of this series of complexes. Indeed, this is the reason why the gadolinium derivative (commercialized as DOTAREM) is one of the most employed contrast agents for magnetic resonance imaging (MRI), alongside with other complexes such as [Gd(DTPA)(H₂O)]²⁻ (DTPA = diethylenetriamine penta-acetic acid). Moreover, ligands derived from DOTA are widely employed and investigated in order to improve selectivity and contrast enhancement.^{6–8}

The exchange of the AWM between the complex and the solvent selectively increases the longitudinal relaxation rate of the water protons in certain tissues,⁹ principle on which the T₁-weighted magnetic resonance imaging (MRI) is based. On the other hand, complexes of the series based on anisotropic lanthanides, like dysprosium, are promising contrast agents for T₂-weighted MRI, a new generation of MRI contrast agents^{10,11} exploiting also new MRI contrast mechanisms such as the

^a Dipartimento di Chimica "U.Schiiff" and UdR INSTM Università degli Studi di Firenze, Via della Lastruccia 3-13, 50019 Sesto Fiorentino (Italy).

^b Université Rennes, CNRS, ISCR (Institut des Sciences Chimiques de Rennes) - UMR 6226, F-35000 Rennes (France).

[†]Present address: Los Alamos National Laboratory, Theoretical Division, Los Alamos, NM 87545, USA.

boris.leguennic@univ-rennes1.fr, federico.totti@unifi.it.

Electronic Supplementary Information (ESI) available: Description of the employed geometrical models; employed ANO-RCC basis sets and contractions; results of the CASSCF-CASSI-SO calculations for all the α and φ angles on all the models (g-tensors of ground and first excited doublets, γ_n angles, energy ladder of the ground J=15/2 multiplet); electrostatic potential maps by CAMMEL for **M1** and **M2m**. See DOI: 10.1039/x0xx00000x



chemical exchange saturation transfer (CEST)¹². The access to the magnetic anisotropy tensor is also an important information to interpret solution and solid-state NMR of paramagnetic proteins. [LnDOTA]⁻ complexes already displayed good qualities in order to assess the structure of proteins by NMR spectroscopy.^{13–15} Indeed, the pseudo-contact shift depends on the position of the atom with respect to the orientation of the magnetic susceptibility tensor and the distance from the paramagnetic center, and its effect is felt on the local environment up to 40 Å.

In the field of molecular magnetism the series of [Ln(DOTA)(H₂O)]⁻ was extensively studied^{3,4} as one of the pioneer complexes of Lanthanide based Single Molecule Magnets (SMMs).¹⁶ SMMs are a class of compounds that present below a certain temperature, called the blocking temperature, T_{block} , slow relaxation of the magnetization and eventually the opening of an hysteresis loop.¹⁷ These properties arise from the electronic structure of the isolated molecule and not from long-range interactions like in classical magnets. The rate of this process is modeled with an Arrhenius-like law $\tau = \tau_0 \exp(U/k_B T)$, where τ is the mean time necessary for the spin to overcome the barrier U . Large efforts were devoted to increase U , the relaxation time and the blocking temperature in order to employ these systems in real devices such as magnetic memories of molecular dimensions,^{18–20} quantum computers,^{21,22} and electronic devices based on molecular spintronic.^{23–25}

The pioneering work of Ishikawa²⁶ demonstrated that in mononuclear complexes containing lanthanide ions anisotropy barriers of hundreds of K could be reached, an order of magnitude higher than the ones observed so far. Generally, the contribution to the coordination bonding of the 4f orbitals, where the unpaired electrons in Ln^{III} ions reside, is not as significant as for the 3d orbitals due to their 'core' character. Therefore, their orbital angular momentum is largely unquenched causing the rise of a magnetic anisotropy of the first order. Despite record energy barriers of thousands of K, the blocking temperatures remained around the temperature of the liquid helium, confirming the complex relation between the anisotropy barrier and the blocking temperature with the geometry. On this topic some light has been shed in some recent papers both for lanthanide and transition metal mononuclear compounds.^{27–31} Very recently, new successful efforts have provided blocking temperatures around the nitrogen boiling point.^{30,32,33} An important contribution to the achievements in the field has been given by computational approaches^{34,35}. In order to rationalize the properties of lanthanide complexes on the computational basis, in the last ten years *ab initio* methods based on Complete Active Space Self Consistent Field³⁶ (CASSCF) with the introduction of the Spin-Orbit (SO) coupling through the Complete Active Space State Interaction³⁷ (CASSI) proved to be able to reproduce experimental findings coming from different experimental techniques as, for instance, DC³⁸ and AC magnetometry,^{39,40} electron paramagnetic resonance,^{41,42} cantilever torque magnetometry,^{39,43,44} inelastic neutron scattering.^{45,46}

However, a clear understanding about some key aspects is still lacking; first of all, a reliable reproduction of the ligand field around the lanthanide ion. In other words, the main problem to face is how to correctly account for the electrostatic field and the covalent interactions between the f orbitals, the ligands and the crystal environment. Indeed, the idea that the 4f orbitals are not strongly involved in the coordination bond as their d orbitals counterpart, supported the idea that a rationalization of the magnetic anisotropy in lanthanide complexes could be based only on electrostatic considerations. Several attempts were made following this idea going from employing formal charges on the ligands⁴⁷ or more sophisticated effective charge models.⁴⁸ The common limitation of these approaches is the underestimation of covalent interactions, which are accountable only with the explicit calculation of the whole electronic structure of the complex. The role of each of the two contributions (covalent and electrostatic) can obviously vary from case to case but even if the former is expected to be, in general, smaller than the latter, the complete neglecting of it can be risky⁴⁹. Indeed, magnetic properties are really sensitive to small perturbations, like tiny deviations from idealized geometry⁴⁹ or variations of the bond distances,^{50,51} i.e. to different combinations of electrostatic and covalent contributions.

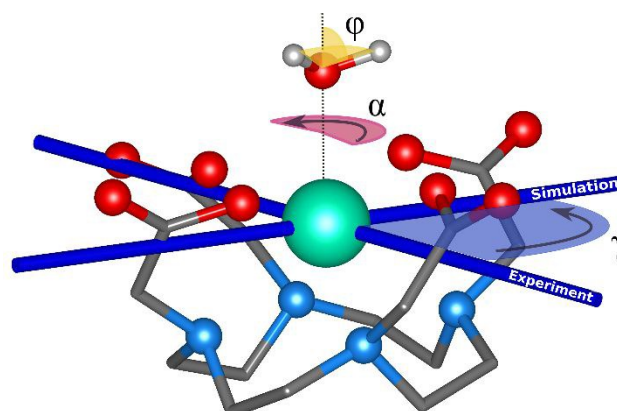


Fig. 1. Main geometrical parameters employed for magneto-structural correlations. α is the angle of rotation around the Dy-O_{AWM} bond; $\theta_{0,1}$ are the angles between the calculated and experimental easy-axis of magnetization for the ground and first excited Kramers' doublets; ϕ is the angle between the Dy-O_{AWM} bond and the plane of the water molecule. Dysprosium atom is coloured in light green, oxygen atoms in red, nitrogen atoms in cyan, carbon atoms in grey and hydrogen AWM atoms in white. Hydrogen atoms of DOTA were not reported for the sake of clarity.

In this framework, not only the employment of the highest affordable level of calculation is necessary but also the choice of the molecular model is crucial because it can seriously affect the results. To make things even more complicated, a reliable reproduction of the crystal environment, i.e. the Madelung potential, becomes another key aspect. To our knowledge, only a few attempts toward such a direction have been done.^{41,52–54} However, these made use of gas-phase computed molecular point charges.

The archetype compound [Dy(DOTA)(H₂O)]⁻ complex (DyDOTA in the following), Fig. 1,² is particularly suitable for the investigation of the interplay of all these contributions. Such a



complex has been deeply characterized both at the computational and experimental level.^{2,4,55} It presents a first coordination sphere with a pseudo-tetragonal symmetry and for this reason either an easy axis of magnetization along the C_4 or an easy-plane behavior in the four coordination DOTA oxygens could be expected. However, DyDOTA presents an easy axis of magnetic anisotropy which is perpendicular to the pseudo-tetragonal axis of the molecule. Interestingly, for the first time, a dependence of the orientation of the main magnetic axis as a function of a tiny structural modification was predicted by *ab initio* methods. Indeed, to reproduce the experimental data (direction and magnitude of the anisotropy axes and the magnetic multiplets energy ladder) a particular orientation of the apical water molecule (AWM)'s hydrogens was necessary. For such a reason, it was supposed an interplay between the electrostatic potential determined by the ligands and a small, but not negligible, covalent interaction between the dysprosium's f orbitals and the AWM's molecular orbitals. This uncommon behavior makes the computational study of this complex a hard but intriguing task. It offers an extraordinary possibility to get insights into how to handle from a computational point of view the subtle equilibrium between covalent contributions and electrostatic field strength.

The different structural modeling proposed in literature led to apparently conflicting results. Both the orientation of the AWM's protons and the extent of the number of atoms explicitly or implicitly considered in the model were analyzed in the original article by Cucinotta *et al.*² The results showed a prominent role of the orientation of the AWM protons in determining the energy ladder and the directions of the anisotropy axes. On the other hand, Chilton *et al.*⁴⁷ showed no influence arising from AWM's orientation on the single ion magnetic anisotropy. The difference in the obtained results resides in the different models employed in the two articles: in particular, the inclusion of distinct coordination spheres surrounding the central $[\text{Dy}(\text{DOTA})(\text{H}_2\text{O})]^-$ cluster, which can strongly affect the electrostatic field's strength.

Summarizing, the aim of this work is double: i) to critically revise the models proposed in literature so far with the aim to give a reliable general approach to model magnetic lanthanide-based complexes as DyDOTA with a better description of the Madelung potential by periodically computed point charges; ii) to shed some light on the perennial question about the interplay between covalent and electrostatic contribution in f-coordination compounds.⁵⁶ To these purposes the magnetic anisotropy tensor - which is a "pure" f orbitals-originated observable - has been used as a reliable probe. It has been here investigated by performing a large variety of magneto-structural correlations involving different structural bonding parameters (rotations, stretching and bending) of the AWM and by an electrostatic multipolar expansion analysis.⁵⁷⁻⁵⁹

This work is focused on a single lanthanide derivative, but the conclusions and the proposed approach can be extended, in general, to other lanthanide based¹⁴ complexes and even beyond the solid state, including MRI's relaxation mechanisms in solution.^{60,61} Indeed, even if in crystals the rotation of the water molecule is not allowed by supramolecular interactions,

in solution this is not true: the water molecule is free to rotate and go through solvent exchange process. This could shed a new light on the mechanism of the relaxation enhancement in solution in presence of MRI contrast agents based on anisotropic lanthanide atoms.

Computational Approach

All employed models are based on crystallographic structural data, with the exclusion of the two H_{AWM} , which have been optimized at the DFT level for **M1** and **M2** models (see below and Computational details). All models are shown and schematically described in Table 1 and Fig. 2 (see ESI for further details). The differences among the presented models rely on the number of explicit atoms considered at the highest computational level (QM) and the eventual addition of a different number of point charges (Table 1). For all of them the same computational protocol CASSCF/CASSI-SO along with all-electron basis sets for all the explicit atoms considered were used (Computational details). Rigid rotations of the apical water molecule were performed on all the presented models.

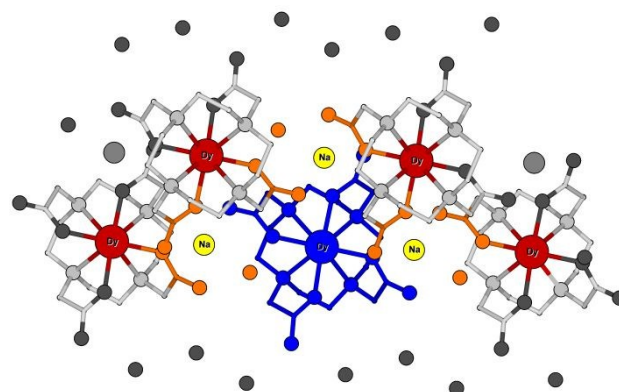


Fig. 2. Scheme of the different models employed. The different colors indicate different parts of the system modeled according to Table 1.

Model 1, **M1** was built based on the necessity to fulfill both chemical soundness (Figs. S1-S2) and an accurate representation of the electrostatic environment around the very sensitive Dy(III) ion. Indeed, the most correct way to model a system as DyDOTA would be considering it in its periodic environment. The problem of this approach is related to the impossibility to perform such a calculation at the level of accuracy affordable by the CASSCF/CASSI-SO approach. To overcome such a problem we mimicked the first four neighbouring $[\text{Dy}(\text{DOTA})(\text{H}_2\text{O})]^-$ units, the counterions and the co-crystallized water molecules with point charges, leaving a single $[\text{Dy}(\text{DOTA})(\text{H}_2\text{O})]^-$ complex explicitly computed at the highest level of accuracy. Due to its *a priori* nature, i.e. without any arbitrary assumption about the extension of the geometry, we have chosen **M1** as our reference model.



Table 1. Summary of the different structural models considered in this paper (**M1-5**) and of the already published ones by Cucinotta *et al.*² The colour's code is referred to Fig. 2.

Models	[DyDOTAH ₂ O] ⁻ (■)	3 Na ⁺ ions surrounding DyDOTA complex (■)	Coord. Sphere of 3 Na ⁺ ions (■)	4 Dy ions of neighbouring molecules (■)	All atoms of 2 neighbouring crystal cells (■)
M1	explicitly QM handled	DDA Point charges	DDA Point charges	DDA Point charges	DDA Point charges
M2/M2m	explicitly QM handled	-	-	-	-
M3	explicitly QM handled	explicitly QM handled	-	-	-
M4	explicitly QM handled	explicitly QM handled	3·(2HCOO ⁻ + H ₂ O)	-	-
M5	explicitly QM handled	explicitly QM handled	3·(2HCOO ⁻ + H ₂ O)	DDA Point charges	-
Cucinotta <i>et al.</i> ² Model A/A'	explicitly QM handled	explicitly QM handled	3·(2HCOO ⁻ + H ₂ O)	explicitly QM mimicked by Na ⁺ ions	-
Cucinotta <i>et al.</i> ² Model C	explicitly QM handled	-	-	-	-
Chilton <i>et al.</i> ⁴⁷	explicitly QM handled	explicitly QM handled	-	-	-

With the aim to reduce the computational effort and consequently testing a reliable but lighter 'operative' model, we reduced **M1** to a different one consisting of only one [Dy(DOTA)(H₂O)]⁻ unit and two aldehydes mimicking the carbonyl groups of an adjacent DyDOTA molecule (Fig. S3). **M2m** differs from the **M2** model by the removal of the two aldehydes. **M2** and **M2m** represent the most intuitive, and therefore, the simplest possible models. By the way, such type of model is widely used in literature when a lanthanide complex is handled at the CASSCF/CASSI-SO level of approximation.^{39,62,63}

In the unit cell, each DyDOTA complex is surrounded by three counter-ions. Model 3 (**M3**) has been designed to account for these three cations at their crystallographic positions (Fig. S4). **M3** was considered because it closely resembles the model used by Chilton *et al.*⁴⁷

Model 4, **M4**, is obtained by adding to **M3** four more formate anions and two water molecules around each of the three Na⁺ ions. The first coordination sphere of each Na⁺ ion is now complete (see also Fig. S5). Finally, to reduce the charge unbalance in **M4**, the computed DFT point charges (Computational details) of the four dysprosium ions belonging to the surrounding complexes were added (Fig. S6) to it (**M5**). Such a model is very close to the Model A/A' (total charge equal to 0) proposed by Cucinotta *et al.*²

Computational Details. Geometry optimization of the positions of the two H_{AWM} in **M1** and **M2** was performed with the quantum chemistry package ORCA⁶⁴. For both models the dihedral angle φ between the plane of the water molecule and the Dy-O_{AWM} bond (see Fig. 1) was computed to be 53.6° and was used throughout all the other models.

Unrestricted DFT/B3LYP⁶⁵ functional together with Van der Waals empirical dispersion correction D3⁶⁶ has been used. VTZPP basis sets for all the atoms were chosen. Relativistic effects were accounted for by using the second-order Douglas-Kroll-Hess (DKH2) Hamiltonian. The spin multiplicity was set to

six. Def2-TZVPP basis set were employed for all the atoms except for the lanthanide atom where SARC-TZV basis⁶⁷ were used.

To simulate the effect of the crystal environment at a larger extent than considering just few neighbouring atoms or pieces of adjacent DyDOTA complexes but still at a computational affordable level, atomic point charges were added to the explicit models. Point charges were computed as density derived atomic point charges (DDAPC)⁶⁸ obtained by a single point calculation on the [NaDy(DOTA)(H₂O)]·4H₂O unit cell using the PBE0 functional⁶⁹ with periodic boundary conditions included. The package of software CP2K⁷⁰ based on a mixed gaussians and plane waves⁷¹ (GPW) formalism was used. Since, basis sets for dysprosium were not available at the time in the package, Dy(III) ions were substituted by La(III) ions. Double- ζ polarized basis sets (mid-PBE for La, DZVP-MOLOPT-SR47 for other atoms) with Goedecker-Teter-Hutter norm conserving pseudopotentials have been employed. The PW cutoff has been set to 400 Ry.

Calculations to estimate excited state energies and the magnetic anisotropy were performed with the package of programs MOLCAS 8.1.⁷² The active space consisted of nine electrons in the seven 4f orbitals of the Lanthanide ion, i.e. CASSCF(9,7).^{73,74} All-electron ANO-RCC⁷⁵⁻⁷⁷ basis sets were employed in all the calculations (see Table S1 for details and contraction schemes). State-average calculations were performed only considering all the sextets (21 roots). Complete Active Space State Interaction (CASSI-SO) was calculated, using the previously computed CASSCF states to check the effect of the spin-orbit splitting on the ground ⁶H_{15/2} ground state. Only the sextets (⁶H, ⁶F, and ⁶P sextets) were taken into consideration since the inclusion of other multiplets did not improve the solution.^{2,38} Moreover, we chose not to include a second order perturbation on top of the CAS solution (CASPT2) since the effect on energy of the first two excited Kramers' doublets was of the order of only few wavenumbers.²



Table 2. Orientation of ground Kramers' doublets main magnetic axis in the molecular frame for the different structural models considered in this paper (M1-5) and for the already published ones. View Article Online
DOI: 10.1039/C9SC01499G

Model	Cucinotta <i>et al.</i> ² (Mod. A) ^a	Cucinotta <i>et al.</i> ² (Mod. A) ^b	Chilton <i>et al.</i> ⁴⁷	M1	M2	M3	M4	M5
$\alpha = 0^\circ$								
γ_0	9.6°	0.6°	~0° ^c	2.8°	8°	5.5°	88°	4.6°
$\alpha = 90^\circ$								
γ_0	85.8°	41.0°	~0° ^c	34.1°	81.1°	3.5°	84°	11.9°
No H ₂ O								
γ_0	7.6°			3.0°	77.5°			

^a Exact Model A in Cucinotta *et al.*² ($\varphi = 0^\circ$)

^b Modified Model A in Cucinotta *et al.*² ($\varphi = 53.6^\circ$)

^c Extracted values from Fig. 3 of Chilton *et al.*⁴⁷ (exact values were not reported).

The main magnetic axes for the first eight Kramers' doublets were computed with the SINGLE-ANISO module⁷⁸ with pseudospin $S = \frac{1}{2}$. γ_0 and γ_1 correspond to the angles between the experimental magnetic easy axis and the computed one for the ground and the first excited Kramers' doublets, respectively (Fig. 1).

The atomic electric multipole moments were computed with the LOPROP module⁷⁹ on the ground state electronic density obtained with the CASSCF/CASSI-SO method. The highly reliable⁸⁰ LOPROP electrostatic charges, dipoles and quadrupoles computed for all the atoms in the DyDOTA models were employed as a basis for the analysis of the electrostatic field around the Ln ion, performed with the homemade CAMMEL (Calculated Molecular Multipolar Electrostatics) code.⁸¹⁻⁸³

Rigid rotation of the two optimized H_{AWM} atoms along the Dy-O_{AWM} axis defines an angle α , whose origin value of 0° corresponds to the optimized H_{AWM} positions and it can vary from 0 to 2π values (Fig. 1). For **M1** and **M2**, α was varied along the whole $[0, 2\pi]$ range. For **M3**, **M4**, and **M5**, calculations were performed only for $\alpha = 0^\circ, 90^\circ$. φ angle has been set to the following values: $0^\circ, 53.6^\circ$, and 90° (see Fig. 1).

Results and Discussions

Rotation of the ground state's easy axis of magnetization

The results obtained for all models for angles $\alpha = 0^\circ, 90^\circ$, and with no AWM, are reported in Table 2 (see also Tables S2-S3). The observed behaviour immediately appears to be strongly model dependent. For **M1** (reference model) the computed g -values for $\alpha = 0^\circ$ show a very good agreement between the experimental and the computed easy axis of magnetization orientations (Figs. 3-4 and Tables S2-S3). The deviation of 3° is well below the experimental uncertainty. However, the role of the AWM seems to be not innocent at all.

Indeed, for $\alpha = 90^\circ$, the easy axis of magnetization remains in the plane containing the DOTA oxygen atoms coordinating the Dy(III) ion but the value of γ_0 is now 34.1° and reaches a maximum of 71.7° (Figs. 3-4) for $\alpha = 120^\circ$. The obtained results show a similar trend with respect to the ones obtained by Cucinotta *et al.*² However, in the latter work, they found the maximal extent of the rotation of the easy axis of magnetization ($\gamma_0 = 85.8^\circ$) for $\alpha = 90^\circ$. Puzzled by these differences, we changed the φ value in the Cucinotta *et al.*'s model from 0° to the optimized one (53.6°), as previously stated in the Computational details: the γ_0 values for $\alpha = 0^\circ$ and 90° changed to 0.6° and 41° , respectively, in very good agreement with **M1** findings. Such results also evidenced how significant the effects deriving from a different geometrical modeling of the AWM can be in the description of the magnetic properties of the system. Moreover, differently from what calculated by Cucinotta *et al.*², by removing the water molecule we observed a γ_0 angle of only 3° .



A completely different approach from **M1** is represented by the choice of **M2**. Indeed, this model represents, along with **M2m** (see SI), the simplest possible model and the most common approach used in literature for Lanthanide-based SMMs, at the same time.^{29,39,63} A similar trend to the one observed for **M1** was found. The main difference resides in the maximal extent of the rotation of γ_0 and the value of α at which it is obtained: 81.1° vs 71.7° (**M1**) and 90° vs 120° (**M1**), respectively. The effect of the removal of the AWM has been studied also for this model. In such a case, the easy axis of magnetization shows a $\gamma_0 = 77.5^\circ$ in agreement with the article by Cucinotta *et al.*²

The results obtained for **M3** are in agreement with the ones reported by Chilton *et al.*⁴⁷: no reorientation of the easy axis of magnetization was observed ($\gamma_0 = 5.5^\circ$ and 3.5° for $\alpha = 0^\circ$ and 90° , respectively). Such result compared to the ones obtained for **M1** and **M2** gives a strong indication on how sensitive to the modeling of its electrostatic environment the Dy(III) ion can be. In this framework, the **M3** model shows a possible bias constituted by the arbitrariness of having three Na⁺ ions with their coordination sphere unsaturated.

To overcome such a bias, **M4** was built to have the Na⁺ ions fully coordinated (see Computational Approach and SI). The non-innocence of such a change in the modeling is witnessed by the results reported in Table 2 and Table S2. Indeed, the easy axis of magnetization was found at γ_0 values of 88° and 84° for $\alpha = 0^\circ$ and 90° , respectively. This means that the addition of the formate ions and of the water molecules has strong effects on the fine magnetic structure of the system, even if they belong only to the second and third coordination spheres of the Dy(III) ion. Such results show, once again, how sensitive the Dy(III) ion can be to the modelling of its electrostatic environment. No reorientation of the easy axis of magnetization, but now with small γ_0 values, was also found for **M5**, which is very close to the Model A/A' proposed by Cucinotta *et al.*² Despite the close similarity, γ_0 values of 4.6° and 11.9° (Tables 2 and S2) were found for $\alpha = 0^\circ$ and 90° , respectively. Instead, a change of orientation of the easy axis of magnetization of about 90° was found for Model A/A' passing from $\alpha = 0^\circ$ to $\alpha = 90^\circ$. Such result confirms once again the strong modeling effects on the fine electronic structure of Dy(III) ion when partial, not to say "arbitrary", models are chosen.

AWM's Influence on the Energy Ladder

Given for granted the role of the AWM in the modulation of the magnetic properties of the DyDOTA, we wanted to shed more light on it, also in the perspective of the more ambitious aim of quantifying the covalent contributions in the Dy-O_{AWM} bond (see next section). We have, therefore, monitored the evolution of the electronic structure of **M1** for twenty values of the α angle. The principal g -values of the ground and first excited Kramers' doublets and the angle between the computed g_z components and the experimental value are reported in Table S4 and Figs. 3-4, respectively.

The computed g -values for $\alpha = 0^\circ$ show a stronger Ising character of the Dy(III) ion than the one experimentally observed but in agreement with the previously computed g -

values by Cucinotta *et al.* (Table S4) and the usual trend reported in literature.^{39,42,80} DOI: 10.1039/C9SC01743G

The ground and the first excited Kramers' doublets show a prominent contribution from the $|M_j\rangle = 15/2$ and $|M_j\rangle = 13/2$ components (ESI and Tables S5-S6) and they are separated by 47 cm⁻¹ in excellent agreement with an experimental value of 52 cm⁻¹. A very good agreement is also evidenced for higher energy doublets which differ from the experimental ones of 16 cm⁻¹ at maximum. Only for E₂ and E₅, a more significant deviance from the luminescence experimental values² was found: deviation of 28 and 31 cm⁻¹, respectively (Table S4). The overall agreement with the experiment is evident. This is not surprising since the present computational model represents so far the most accurate representation of the

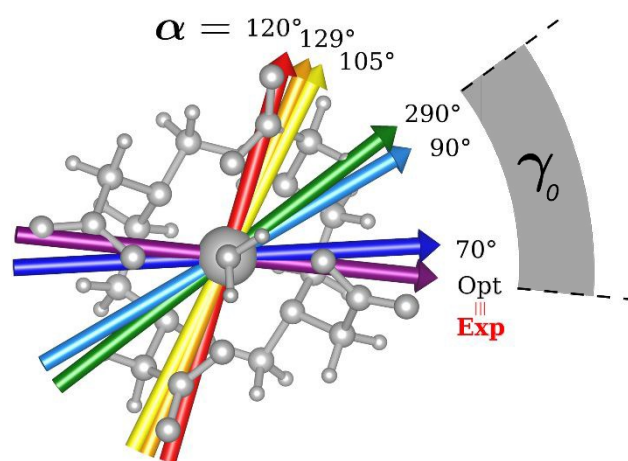


Fig. 3. Model **M1**. Computed ground state's easy axis for different α angles inside the molecular frame.

environment that a single [Dy(DOTA)(H₂O)]⁻ unit can experience. In a nutshell, the geometrical and chemical arbitrariness were reduced to the minimum in this model. Interestingly, the first excited Kramers' doublet shows also a significant Ising character and the orientation of its g_z component is quasi-orthogonal (80.1°) to the one of the ground doublet.



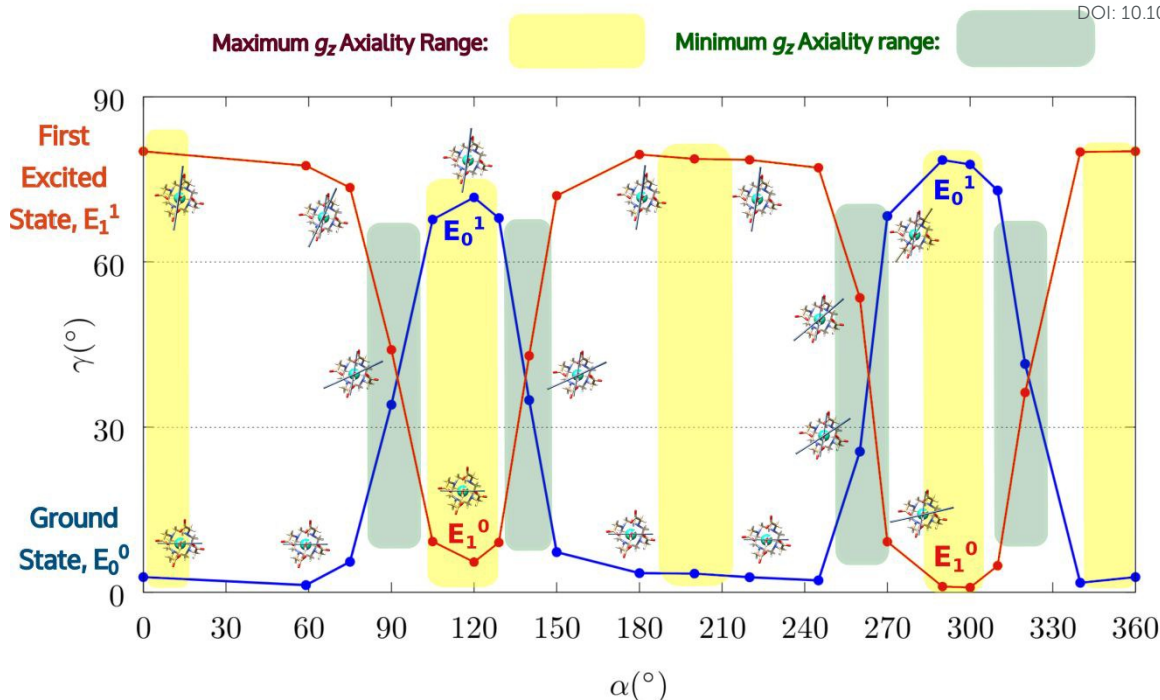


Fig. 4. Model M1. Variation of the angle $\gamma_{0,1}$ as a function of the rotation of the AWM (α), for ground and first excited states.

Encouraged by these results, we have performed the same calculations for different α values. First of all, we have tried to calculate the evolution of the orientation of the easy axis of magnetization for $0^\circ < \alpha < 90^\circ$ as already reported in literature^{2,47} (Figs. 3-4 and Table S4) and then extended to $90^\circ < \alpha < 360^\circ$. The choice to extend the α range is due to the asymmetry introduced by the presence of the two carboxylate groups coordinating the H_{AWM} atoms in the explicit [Dy(DOTA)(H₂O)]⁻ unit. For more clarity, the g_z orientations as a function of the α angle are collected for both the ground and the first excited Kramers' doublet in Figs. 3 and 4. Regarding the ground state (blue curve in Fig. 4), the value of γ_0 remains almost constant up to $\alpha = 60^\circ$ and, only beyond this value, it increases up to its maximum value of $\gamma_0 = 71.7^\circ$ computed for $\alpha = 120^\circ$. Therefore, the easy axis orientation change can be considered as a smooth process since a range of 60° is needed by the angle α to cover the gap between the minimum and maximum γ_0 values. Moreover, the easy magnetization axis took about 60° ($\alpha = 180^\circ$) to recover a value of γ_0 close to 0° .

A similar trend is observed also for $180^\circ < \alpha < 360^\circ$, even if a slightly higher maximum was achieved ($\gamma_0 = 78.5^\circ$) maintaining practically unaltered the range of α values for which the variation of γ_0 takes place.

Such results are important for two main reasons: first, they show that a strong reorientation of the easy axis of magnetization can be induced by the simple rotation of the AWM but at larger values than $\alpha = 90^\circ$, in contradiction to what was reported by previous models.^{2,47} Secondly, the reorientation is a smooth phenomenon and not an abrupt one as reported in Cucinotta *et al.*², where the change in the orientation of γ_0 was observed within 15° of the α angle: γ_0 passed from $\sim 1^\circ$ to 92° from $\alpha = 45^\circ$ to $\alpha = 60^\circ$. Only changing φ

to the Cucinotta *et al.* value, we can recover the abrupt switch between E_0 and E_1 doublets.

It is also worth to stress that similar results, but opposite in trend, were obtained for the first excited Kramers' doublet. Interestingly, the sum of the two $\gamma_{0,1}$ values observed for the ground and the first Kramers' doublet state, respectively, is found to be constant ($80^\circ \pm 3^\circ$) for all the 2π range. On this basis, we can theorize that E_0 goes toward a swapping process with E_1 depending on the rotation angle of the water molecule. From an accurate analysis of the energy ladders calculated for different α angle values, such a flipping process between the two first Kramers' doublets can be rationalized in three main steps (Fig. 5).

In the first step, where α values range between 0° and 70° , the rotation of the water molecule alone induces a destabilization of E_0 of about $20\text{--}25\text{ cm}^{-1}$ (E_{rot1}), leaving the energy ladder practically unchanged for $E_2\text{--}E_7$ (a rigid stabilizing shift of $20 \pm 3\text{ cm}^{-1}$ is observed, see Table S4). On the contrary, the energy of the first excited Kramers' doublet, E_1 , remains practically constant. In this α range, both E_0 and E_1 keep their easy magnetic axis original orientation ($2.8^\circ < \gamma_0 < 5.5^\circ$ and $73.5^\circ < \gamma_1 < 80.1^\circ$).

In the second step, that is for $70^\circ < \alpha < 90^\circ$, we observed a kind of avoided crossing scenario between E_0 and E_1 states. This is witnessed by the fact that for $\alpha = 90^\circ$ we have an intermediate easy axis orientation both for the ground and the first excited Kramers' doublet ($\gamma_0 = 34.1^\circ$ and $\gamma_1 = 44.0^\circ$, respectively). Being for this α angle the composition of the two Kramers' doublets very similar (Tables S5-S6), the E_0 and E_1 related energy surfaces undergo to an avoided crossing state. We can qualitatively estimate $E_{cross} \sim 20\text{ cm}^{-1}$.⁸⁴



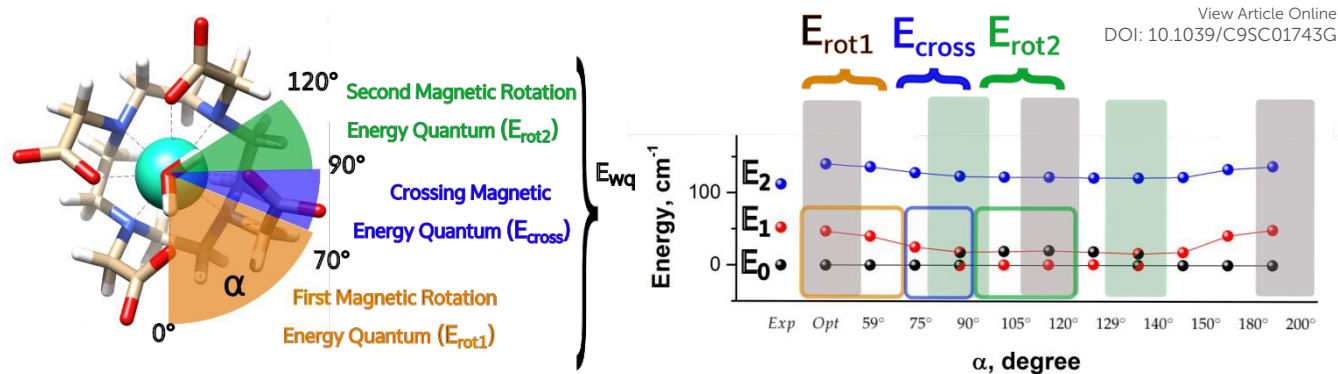


Fig. 5. Energetic variations involving the ground and first excited Kramers' doublet as a function of the AWM's angle of rotation α for **M1**.

In the third step, where α values range between 90° and 120° , the involved energies are the ones needed to re-flip the two Kramers' doublets states and make their composition similar to their original ones with their easy axes of magnetization quasi-orthogonal again ($67.7^\circ < \gamma_0 < 71.7^\circ$, $9.2^\circ < \gamma_1 < 5.5^\circ$). In this regard, it is not surprising that an E_{rot2} value equal to the one obtained for $0^\circ < \alpha < 70^\circ$ is found. From the considerations above, we can say that the energy quantum involved to reach the avoided crossing point ($E_{rot1} + E_{cross}$) is about $40\text{--}50\text{ cm}^{-1}$. The needed energy to completely rotate the easy magnetization axis ($E_{rot1} + E_{cross} + E_{rot2}$) can be, therefore, estimated in about $60\text{--}70\text{ cm}^{-1}$. Such result suggests that in the case the separation energy between the first two Kramers' doublets would exceed the requested flip energy quantum ($40\text{--}50\text{ cm}^{-1}$), the reorientation of the easy axis of magnetization would not likely take place. Of course, the value of the energy flip quantum could be model dependent, but the physics under the phenomenon is valid in general (*vide infra*). Unexpectedly, in the $90^\circ < \alpha < 140^\circ$ range, in correspondence of the flip of the easy axis of magnetization from $\gamma_0 \sim 0^\circ$ to 72° and back to 35° , the $E_0\text{--}E_7$ energies show very small variations ($1\text{--}3\text{ cm}^{-1}$). This can be explained by the fact that the two doublets are not completely flipped, except for $\alpha = 120^\circ$. From $\alpha = 150^\circ$, a new flip between the first two doublets was observed, leading to values of γ_0 and doublets ladder energies for $\alpha = 200^\circ$, which correspond to the ones computed for $\alpha = 0^\circ$ (Table S4). From this α value, the ground doublet energy started to be destabilized again by the further AWM rotation until to when, for $\alpha = 260^\circ$, a further flip of the easy axis of magnetization was computed. In the range $270^\circ < \alpha < 320^\circ$, $E_0\text{--}E_7$ energies were computed very close to the corresponding energies found for the $90^\circ < \alpha < 140^\circ$ range.

From the present results the pivotal importance of periodic contributions clearly emerges, hence treated only at an electrostatic level and with an indirect inclusion. Their introduction revealed, indeed, a richer electronic structure than the one observed in simpler models. The analysis made so far can give a hint on the reason why different models in literature did not show any changes in the orientation of the easy axis of magnetization in function of the variation of α : all depends on the computed deviation from the experimental $E_0\text{--}E_1$ gap. Indeed, since the rotation of the AWM requires an energy of about $60\text{--}65\text{ cm}^{-1}$ going from $\alpha = 0^\circ$ to $\alpha = 120^\circ$, in the case the computed gap is larger than $60\text{--}70\text{ cm}^{-1}$, no flip of the easy axis

will be likely observed (see Chilton *et al.*⁴⁷); in the case the gap is smaller, the ground doublet can be erroneously computed due to a poor geometrical modeling choice, thus leading to a partial or total prevalence of wrong orientation of the easy axis of magnetization (**M3-5**). It becomes evident that the modeling of lanthanide systems needs considerable care to avoid unwanted misinterpretation of the experimental findings.

The effect on the energy ladder due to the removal of the AWM was also studied. Focusing on the energy values of the ground and the first excited Kramers' doublets, a shift of the latter by 20 cm^{-1} was observed (see Table S3).

With the aim to verify the influence of the model on the electronic and magnetic structure, we have studied **M2** (and its derived **M2m**) at the same extent of **M1** calculating the evolution of the electronic structure for eighteen values of α (Tables S7-S8 and Figs. S7-S9). Despite an apparent similarity to **M1**, slight but important differences in the electronic structure can be noted. In agreement with **M1**, the rotation effect on the flip of the easy axis is fully confirmed as its Ising type along all the α values, even if the rhombicity is more enhanced than in **M1** and, therefore, in even nicer agreement with the experiment. The deviation of 8° from the experimental orientation of the g_z values is below experimental uncertainty. As for **M1**, the ground and the first excited Kramers' doublets show a prominent contribution from the $|M_j\rangle = 15/2$ and $|M_j\rangle = 13/2$, but in this case, they are separated by only 15 cm^{-1} versus an experimental value of 53 cm^{-1} . In this case ($E_{rot1} + E_{cross}$) is $\sim 40\text{ cm}^{-1}$, in good agreement with the value found in **M1** model. The maximum flip is now reached in a narrower α range ($0^\circ < \alpha < 90^\circ$) and the flip can happen at lower α values (45°) than in **M1** because in this case E_{rot1} and $E_0\text{--}E_1$ are comparable. Even for this model the two $\gamma_{0,1}$ values are nearly complementary ($77^\circ \pm 13^\circ$) as observed in **M1** for all α values. The effect of φ on the first four excited Kramers' doublets is limited to a ten of cm^{-1} (see Tables S9-S10).

The effect of the removal of the water molecule has been studied also for this model (Table S3). The energy separation between the ground and the first excited Kramers' doublets is equivalent to the one found for **M1** without AWM. However, in this case, the easy axis of magnetization showed a $\gamma_0 = 77.5^\circ$ in agreement with Cucinotta *et al.*² Such a result further stresses the model dependency of magnetic properties.



Based on the above analysis, it becomes straightforward to rationalize the different computed effect of the AWM on the easy axis orientation in the other models and in the ones already reported in the literature. Indeed, the absence of easy axis' rotation in **M3** can now be explained by the computed large E_0-E_1 separation with respect to the $(E_{\text{rot1}}+E_{\text{cross}})$ quantum involved in the AWM rotation, preventing, *de facto*, the flip between the two states for the entire range of α values, 90° included.

In the case of **M4**, we have instead a situation where the ground state is flipped with the first excited one for all the α angle values. This means that the inclusion of the formate ions and the water molecules in the second-third coordination spheres of the Dy(III) ion, is not negligible at all because it strongly stabilizes the Kramers' doublet characterized by a perpendicular orientation of the easy axis with respect to the experimental one becoming the ground state even for $\alpha = 0^\circ$. In **M5** the effect of the model choice (inclusion of point charges) is opposite and it always stabilizes the doublet characterized by a close orientation of the easy axis to the experimental one.

Analyzing the computed energy values for the first eight multiplets of **M3-5** models (Table S2) several important information can be extracted (for a more detailed discussion see SI). First of all, comparing the computed trends for the ground and the first excited Kramers' doublets for the three models, it results that the rotation of the AWM has opposite effects on them: strongly destabilizing the former and slightly stabilizing the latter. Moreover, the energy required for the AWM rotation in the range $0^\circ < \alpha < 90^\circ$, i.e. $(E_{\text{rot1}}+E_{\text{cross}})$, is consistently found $40 \pm 3 \text{ cm}^{-1}$ to be for all the models.

About the nature of Dy-O_{AWM} bond

Focusing on the nature of the coordinative bond in lanthanide complexes, the periodic computed trend of the variation of the doublets energy ladder as a function of the α value, suggested

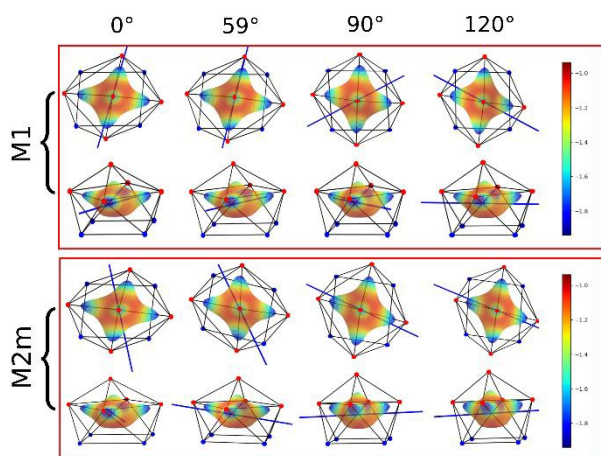


Fig. 6. Electrostatic potential computed by CAMMEL for **M1** and **M2m** at different α angles. For each α angle, top and side views of the complex are shown. Only the atoms directly bonded to the Dy(III) ion are shown. Oxygen and nitrogen atoms are red and blue, respectively. The orientation (blue line) of the easy axis of magnetization for each geometry is also shown.

that the interaction between the Dy(III) ion and the water

molecule could hide a more complex “courtship ritual” than the expected one given by simple electrostatic interactions. For these reasons, we performed a series of further calculations aimed at shedding light on this appealing topic.

The common assumption is that the electrostatic interactions, due to the inner nature of f orbitals, are the main responsible of the ligand field effects in lanthanides containing complexes and, therefore, their magnetic properties are strongly dependent by them. Thus, we have performed a multipolar electrostatic analysis on **M1** and **M2m** through which it has been possible to access the single charge, dipolar and quadrupolar contributions to the electrostatic potential. This analysis has been performed using the CAMMEL code for four α values ($0^\circ-59^\circ-90^\circ-120^\circ$). We have chosen these two models, i.e. the most accurate one versus the simplest one, to have clearer indications without any loss of generality.

The results of the CAMMEL analysis for both models are reported in Fig. 6 and Figs. S10-S17. They indicate the presence of four minima in the whole electrostatic potential which point toward the four coordinating carboxylic oxygen atoms. From the multipolar decomposition, it is possible to ascribe the presence of minima to the dipolar and quadrupolar components, while the contribution generated by the charges shows, instead, a more isotropic shape. Such a scenario does not show any appreciable differences for both considered models and the corresponding α sets of values. It clearly indicates that the electrostatic environments show two equivalent preferential orientations for the easy axis of magnetization, which qualitatively correspond to the computed directions of the first two doublets. However, the analysis cannot give any indication on which of the two directions can be the one associated to the ground doublet.

From the analysis of the plots reported in Figs. 6 and S10-S17, it is not possible to grasp any evident information regarding the AWM subtle role. In this regard, we have tried to extrapolate the single electrostatic contributions of AWM by plotting the difference between the potentials calculated for **M1** and its counterpart without the AWM for the two sets of α values. In both cases, we can observe that the quadrupolar potential represents the strongest electrostatic contribution as expected for a water molecule⁸⁵ (Fig. S18), but a variation of the potential as a function of the α values is observed only for the dipolar component. To verify if eventual variations for the quadrupolar potentials could be hidden by isotropic contributions, we have also re-plotted the maps differences subtracting the AWM potential previously obtained for $\alpha = 0^\circ$ as reference (Fig. S19). The new plots evidenced a variation in the potential also for the quadrupolar contribution and this variation is of the same order of magnitude of the dipolar component. In a nutshell, we can expect that the electric quadrupolar field of the water molecule should have a major role in the re-orientation mechanism of the easy axis of magnetization while a minor role is expected for the dipole. In the case of the charge, we can exclude any significant role in it.

Strong of such results, we tried to put them on a more accurate computational basis. With this aim, we have performed CASSCF/CASSI-SO calculations for **M1** for the same $0^\circ-90^\circ-120^\circ$



set of α values substituting the AWM atoms with their multipolar expansion (**M1**[#]). With such a “trick” we can access to the whole and the single electrostatic contributions and readily verify their effects on the energy ladder and, consequently, on the orientation of the easy axis of magnetization. The results are reported in Table S11. The results obtained for **M1**[#] indicate that the whole electrostatic contribution coming from the AWM is able to rotate the easy axis but not completely ($\gamma_0 = 46.3^\circ$), as found when the AWM is explicitly considered ($\gamma_0 = 71.7^\circ$). Comparing the E_0 and E_1 values for the $\alpha = 0^\circ$ and 120° it is then possible to assign a new easy axis energy quantum of $\sim 65 \text{ cm}^{-1}$ ($E_{\text{rot1}}^{\#} + E_{\text{cross}}^{\#}$). Such an energy

point charges' electrostatic field ($15\% \gamma_0 = 6.5^\circ$) while the dipole moment has only a minor effect. In this regard, to support the previous clues, we have performed CASSCF/CASSI-SO calculations for **M1** and **M1**[#] for $\alpha = 120^\circ$, where we have stretched the Dy-O_{AWM} bond for a maximum of 0.2 \AA , as reported in Table 3. The choice of the $\alpha = 120^\circ$ is justified by the fact that the removal (i.e. extreme stretching situation) of the water molecule in **M1** leads to $\gamma_0 = 4^\circ$. Therefore, stretching the Dy-O_{AWM} for $\alpha = 120^\circ$ geometry we can get further hints about the nature of the bonding and the factors ruling the rotation of the easy axis. Focusing on the energy trends of E_0 and E_1 , we can observe that,

DOI: 10.1039/C9SC01743G

Table 3. Results of the calculations on model **M1**, in function of the Dy-O_{AWM} stretching (in Angstrom) for the rotation of $\alpha = 120^\circ$. Calculations substituting the AWM with its multipole expansion have been also performed.

	0 Å			0.05 Å		0.1 Å		0.15 Å		0.2 Å		noH ₂ O
	Exp	Orb	Charges	Orb	Charges	Orb	Charges	Orb	Charges	Orb	Charges	
Principal g -values of the ground Kramer's doublet												
g_x	3.4	0.9	0.5	0.9	0.6	1.0	0.7	1.0	0.7	1.0	0.7	0.6
g_y	4.9	4.1	1.8	5.0	3.5	5.8	3.9	6.5	4.0	6.9	3.8	2.9
g_z	17.0	16.0	14.6	15.1	14.6	14.3	15.0	13.7	15.4	13.3	15.8	17.3
γ_0 Angle between experimental and calculated g_z												
		71.7°	46.3°	67.7°	29.1°	62.0°	19.2°	54.2°	14.2°	44.7°	11.2°	3.0°
Energy levels (cm^{-1})												
E_0	0	0	0	0	0	0	0	0	0	0	0	0
E_1	52	20	6	18	7	17	8	16	10	16	11	27
E_2	112	122	97	122	101	123	106	123	109	124	112	146
E_3	198	194	144	193	152	193	159	193	166	194	171	231
E_4	287	281	229	283	239	285	249	288	257	291	265	356
E_5	400	351	298	359	316	367	332	376	346	384	359	506
E_6	454	430	378	448	405	465	431	482	453	499	473	702
E_7	574	566	470	595	515	622	557	648	593	673	625	982

value can therefore explain the computed intermediate γ_0 value since the starting E_1 is at 58 cm^{-1} , which is too high in energy to observe a complete flip. Interestingly, the computed ($E_{\text{rot}}^{\#} + E_{\text{cross}}^{\#}$) energie for **M1**[#] is the same energy which was previously found in **M1** model for ($E_{\text{rot1}} + E_{\text{cross}} + E_{\text{rot2}}$).

The expressions for the two energies describe, indeed, the same process: the only difference is that while for the former a total localization of the state is possible ($E_{1,\alpha=0^\circ} < 50 \text{ cm}^{-1}$), for the latter the localization is not possible because $E_{1,\alpha=0^\circ} > 50 \text{ cm}^{-1}$. Such result is important because it demonstrates that the rotation of the easy axis is in large part driven by an electrostatic constant energy quantum. At the same time, it must be stressed once again the cruciality of having an accurate description of the energy ladder. This is possible only when covalent contributions are included and a reliable environment is modeled, too. The fingerprint of covalent contributions can be hinted by looking at the magnetic easy axis computed for $\alpha = 0^\circ$, where, indeed, a difference in γ_0 of 4° has been found. On the other hand, the difference in the energy ladders is significant.

Based on such evidences, we have also investigated the eventual different roles of the electrostatic potential using **M1**[#]. The results are reported in Table S12. In agreement with the pure electrostatic approach, the driving force of the easy axis rotation is mainly due to the quadrupolar (80%, $\gamma_0 = 36.2^\circ$) and

when the orbital contributions for the AWM are included, the E_1 values got stabilized as the Dy-O_{AWM} bond got stretched. This is an expected behavior since the system tends toward the situation where the AWM is absent, and, therefore, to a situation where E_1 flips with E_0 in the range $70^\circ < \alpha < 90^\circ$.

Associated to the E_1 stabilization we can also observe a decrease of the γ_0 values. An opposite situation is found for **M1**[#]: in this case E_1 energies get destabilized as the Dy-O_{AWM} bond got stretched. Such result indicates that in **M1**[#] for $\alpha = 120^\circ$, E_0 and E_1 are already flipped. For this reason, we can observe a similar trend of the E_1 destabilization as in **M1** but associated to a sudden γ_0 decrease, while in **M1** a smoother decrease (overlap vs coulomb interaction) was found.

Under the light of the previous clues, considering that in **M1**[#] for $\alpha = 120^\circ$ E_0 and E_1 are already flipped, we can reconsider the nature of the ($E_{\text{rot1}}^{\#} + E_{\text{cross}}^{\#}$) energy quantum. Indeed, comparing the $E_0 - E_1$ energy splitting (20 and 6 cm^{-1} for **M1** and **M1**[#], respectively) obtained for $\alpha = 0^\circ$, we can now confidently say that the energy quantum of AWM rotation can be divided in $\sim 50 \text{ cm}^{-1}$ (75%) coming from an electrostatic contribution and $\sim 15 \text{ cm}^{-1}$ (25%) from an orbital contribution. Such a value is also compatible with the difference of few degrees computed for **M1** and **M1**[#] at $\alpha = 0^\circ$. Such results undoubtedly indicate that that the covalent contribution is much more relevant than estimated before for Ln-halides bonds and, consequently, that



the orientation of the easy axis is the result of the complex balancing between electrostatic and covalent contributions. 53,56

Conclusions

We have performed exhaustive state-of-art computational analysis of the role of the AWM in tuning the magnetic properties in a very actual compound, as DyDOTA is both for its archetype role in molecular magnetism and its application as MRI contrast agent. The proposed approach and the conclusions presented herein can be extended in general, to other lanthanide based¹⁴ complexes and even beyond the solid state, including MRI's relaxation mechanisms in solution.

Our study allowed to disentangle the different outcomes of previous works presented in the literature, demonstrating that the DyDOTA's behaviour is unique and depends on the correct representation of the crystallographic environment (i.e. Madelung potential) and the AWM itself. Once they are correctly represented in the *in silico* experiment, we showed that the rotation of the AWM effectively strongly influences the orientation of the easy axis of magnetization for a maximum value of 70° with a smooth process. Moreover, we demonstrated that the rotation of the easy axis is due to the flipping of the ground doublet with the first excited one. Therefore, the accurate calculation of this gap, $\Delta(E_1-E_0)$, becomes mandatory. In these regards, we were also able to quantify the energy flip quantum, E_{wq} , in ~ 65 cm⁻¹. Consequently, only in the case the $\Delta(E_1-E_0)$ is smaller than the E_{wq} , the two first doublets can flip and the orientation of the easy axis with them.

Such deep analysis gave us also the opportunity to get an unprecedented information about the nature of the Dy-O_{AWM} bond. Indeed, through electric multipolar expansion analysis and *ab initio* magneto-structural correlations, we got to the conclusions that electrostatic contributions are not enough to explain the rotation of the easy axis and that the quadrupolar potential is its main driving force. At last, but not least, we showed that a clear and crucial covalent footprint is present and it can be quantified as $\sim 25\%$ of the Dy-O_{AWM}.

Conflicts of interest

There are no conflicts to declare.

Acknowledgements

We acknowledge the financial contribution of the ERC through the AdG MolNanoMas (267746). B.L.G. thanks the French GENCI/IDRIS-CINES center for high-performance computing resources.

Notes and references

1 P. Caravan, J. J. Ellison, T. J. McMurphy and R. B. Lauffer,

Chem. Rev., 1999, **99**, 2293–2352.

- 2 G. Cucinotta, M. Perfetti, J. Luzon, M. Etienne, P.-E. Car, A. Caneschi, G. Calvez, K. Bernot and R. Sessoli, *Angew. Chem., Int. Ed.*, 2012, **51**, 1606–1610.
- 3 M.-E. Boulon, G. Cucinotta, J. Luzon, C. Degl'Innocenti, M. Perfetti, K. Bernot, G. Calvez, A. Caneschi and R. Sessoli, *Angew. Chem, Int. Ed.*, 2013, **52**, 350–4.
- 4 P.-E. Car, M. Perfetti, M. Mannini, A. Favre, A. Caneschi and R. Sessoli, *Chem. Comm.*, 2011, **47**, 3751–3753.
- 5 J. F. Desreux, *Inorg. Chem.*, 1980, **19**, 1319–1324.
- 6 K. Kumar, C. A. Chang, L. C. Francesconi, D. D. Dischino, M. F. Malley, J. Z. Gougoutas and M. F. Tweedle, *Inorg. Chem.*, 1994, **33**, 3567–3575.
- 7 S. Aime, A. Barge, M. Botta, D. Parker and A. S. De Sousa, *J. Am. Chem. Soc.*, 1997, **119**, 4767–4768.
- 8 O. A. Blackburn, N. F. Chilton, K. Keller, C. E. Tait, W. K. Myers, E. J. L. McInnes, A. M. Kenwright, P. D. Beer, C. R. Timmel and S. Faulkner, *Angew. Chem, Int. Ed.*, 2015, **54**, 10783–10786.
- 9 K. Micskei, L. Helm, E. Brucher and A. E. Merbach, *Inorg. Chem.*, 1993, **32**, 3844–3850.
- 10 T. C. Soesbe, S. J. Ratnakar, M. Milne, S. Zhang, Q. N. Do, Z. Kovacs and A. D. Sherry, *Magn. Reson. Med.*, 2014, **71**, 1179–1185.
- 11 X. Y. Zheng, J. Pellico, A. A. Khrapitchev, N. R. Sibson and J. J. Davis, *Nanoscale*, 2018, **10**, 21041–21045.
- 12 S. Viswanathan, Z. Kovacs, K. N. Green, S. J. Ratnakar and A. D. Sherry, *Chem. Rev.*, 2010, **110**, 2960–3018.
- 13 B. Graham, C. T. Loh, J. D. Swarbrick, P. Ung, J. Shin, H. Yagi, X. Jia, S. Chhabra, N. Barlow, G. Pintacuda, T. Huber and G. Otting, *Bioconjug. Chem.*, 2011, **22**, 2118–2125.
- 14 L. Benda, J. Mares, E. Ravera, G. Parigi, C. Luchinat, M. Kaupp and J. Vaara, *Angew. Chem, Int. Ed.*, 2016, **55**, 14713–14717.
- 15 S. Dasgupta, X. Hu, P. H. J. Keizers, W. M. Liu, C. Luchinat, M. Nagulapalli, M. Overhand, G. Parigi, L. Sgheri and M. Ubbink, *J. Biomol. NMR*, 2011, **51**, 253–263.
- 16 (a) S. T. Liddle and J. van Slageren, *Chem. Soc. Rev.*, 2015, **44**, 6655–6669; (b) P. Zhang, L. Zhang and J. Tang, *Dalton Trans.*, 2015, **44**, 3923–3929; (c) Z. Zhu, M. Guo, X.-L. Li and J. Tang, *Coord. Chem. Rev.*, 2019, **378**, 350–364; (d) P. Zhang, L. Zhang, C. Wang, S. Xue, S.-Y. Lin and J. Tang, *J. Am. Chem. Soc.*, 2014, **136**, 4484–4487.
- 17 D. Gatteschi, R. Sessoli and J. Villain, *Molecular Nanomagnets*, OUP Oxford, 2011.
- 18 M. Mannini, F. Pineider, P. Sainctavit, C. Danieli, E. Otero, C. Sciancalepore, A. M. Talarico, M. Arrio, A. Cornia, D. Gatteschi and R. Sessoli, *Nat. Mater.*, 2009, **8**, 194–197.
- 19 M. Mannini, F. Pineider, C. Danieli, F. Totti, L. Sorace, P. Sainctavit, M. Arrio, E. Otero, L. Joly, J. C. Cezar, A. Cornia and R. Sessoli, *Nature*, 2010, **468**, 417–21.
- 20 F. E. Kalkf, M. P. Rebergen, E. Fahrenfort, J. Girovsky, R. Toskovic, J. L. Lado, J. Fernández-Rossier and A. F. Otte, *Nat. Nanotechnol.*, 2016, **18**, 926–929.
- 21 D. Aguila, L. A. Barrios, V. Velasco, O. Roubeau, A. Repolles, P. J. Alonso, J. Sese, S. J. Teat, F. Luis, G. Aromi and J. Pablo, *J. Am. Chem. Soc.*, 2014, 14215–14222.
- 22 M. Shiddiq, D. Komijani, Y. Duan, A. Gaita-Ariño, E. Coronado and S. Hill, *Nature*, 2016, **531**, 348–351.
- 23 S. Sanvito, *Chem. Soc. Rev.*, 2011, **40**, 3336.
- 24 R. Vincent, S. Klyatskaya, M. Ruben, W. Wernsdorfer and F. Balestro, *Nature*, 2012, **488**, 357–360.
- 25 M. Ganzhorn, S. Klyatskaya, M. Ruben and W. Wernsdorfer,



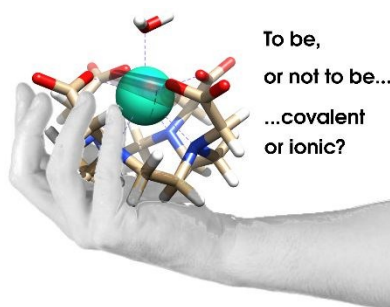
- Nat. Nanotechnol.*, 2013, **8**, 165–169.
- 26 N. Ishikawa, M. Sugita, T. Ishikawa, S. Koshihara and Y. Kaizu, *J. Am. Chem. Soc.*, 2003, **125**, 8694–8695.
- 27 A. Lunghi, F. Totti, R. Sessoli and S. Sanvito, *Nat. Commun.*, 2017, **8**, 14620.
- 28 A. Lunghi, F. Totti, S. Sanvito and R. Sessoli, *Chem. Sci.*, 2017, **8**, 6051–6059.
- 29 C. A. P. Goodwin, F. Ortu, D. Reta, N. F. Chilton and D. P. Mills, *Nature*, 2017, **548**, 439–442.
- 30 F. Guo, B. M. Day, Y. Chen, M. Tong, A. Mansikkamäki and R. A. Layfield, *Science*, 2018, **362**, 1400–1403.
- 31 P. C. Bunting, M. Atanasov, E. Damgaard-Møller, M. Perfetti, I. Crassee, M. Orlita, J. Overgaard, J. van Slageren, F. Neese and J. R. Long, *Science*, 2018, **362**, eaat7319.
- 32 C. A. P. Goodwin, F. Ortu, D. Reta, N. F. Chilton and D. P. Mills, *Nat. Publ. Gr.*, 2017, **548**, 439–442.
- 33 F. S. Guo, B. M. Day, Y. C. Chen, M. L. Tong, A. Mansikkamäki and R. A. Layfield, *Angew. Chem., Int. Ed.*, 2017, **56**, 11445–11449.
- 34 N. F. Chilton, *Inorg. Chem.*, 2015, **54**, 2097–2099.
- 35 L. Ungur and L. F. Chibotaru, *Phys. Chem. Chem. Phys.*, 2011, **13**, 20086.
- 36 B. O. Roos and P.-Å. Malmqvist, *Phys. Chem. Chem. Phys.*, 2004, **6**, 2919.
- 37 P. A. Malmqvist, B. O. Roos and B. Schimmelpfennig, *Chem. Phys. Lett.*, 2002, **357**, 230–240.
- 38 K. Bernot, J. Luzon, L. Bogani, M. Etienne, C. Sangregorio, M. Shanmugam, A. Caneschi, R. Sessoli and D. Gatteschi, *J. Am. Chem. Soc.*, 2009, **131**, 5573–5579.
- 39 E. Lucaccini, M. Briganti, M. Perfetti, L. Vendier, J.-P. Costes, F. Totti, R. Sessoli and L. Sorace, *Chem. - A Eur. J.*, 2016, **22**, 5552–5562.
- 40 (a) E. Rousset, M. Piccardo, M. E. Boulon, R. W. Gable, A. Soncini, L. Sorace and C. Boskovic, *Chem. - A Eur. J.*, 2018, **24**, 14768–14785; (b) Y.-N. Guo, L. Ungur, G. E. Granroth, A. K. Powell, C. Wu, S. E. Nagler, J. Tang, L. F. Chibotaru and D. Cui, *Sci. Rep.*, 2014, **4**, 5471.
- 41 K. S. Pedersen, L. Ungur, M. Sigrist, A. Sundt, M. Schau-Magnussen, V. Vieru, H. Mutka, S. Rols, H. Weihe, O. Waldmann, L. F. Chibotaru, J. Bendix and J. Dreiser, *Chem. Sci.*, 2014, **5**, 1650.
- 42 R. Marx, F. Moro, M. Dörfel, L. Ungur, M. Waters, S. D. Jiang, M. Orlita, J. Taylor, W. Frey, L. F. Chibotaru and J. van Slageren, *Chem. Sci.*, 2014, **5**, 3287.
- 43 M. Perfetti, M. A. Sørensen, U. B. Hansen, H. Bamberger, S. Lenz, P. P. Hallmen, T. Fennell, G. G. Simeoni, A. Arauzo, J. Bartolomé, E. Bartolomé, K. Lefmann, H. Weihe, J. van Slageren and J. Bendix, *Adv. Funct. Mater.*, 2018, **28**, 1801846.
- 44 M. A. Sørensen, U. B. Hansen, M. Perfetti, K. S. Pedersen, E. Bartolomé, G. G. Simeoni, H. Mutka, S. Rols, M. Jeong, I. Zivkovic, M. Retuerto, A. Arauzo, J. Bartolomé, S. Pilgkos, H. Weihe, L. H. Doerrer, J. Van Slageren, H. M. Rønnow, K. Lefmann and J. Bendix, *Nat. Commun.*, 2018, **9**, 1292.
- 45 M. Voonci, M. J. Giansiracusa, W. Van Den Heuvel, R. W. Gable, B. Moubaraki, K. S. Murray, D. Yu, R. A. Mole, A. Soncini and C. Boskovic, *Inorg. Chem.*, 2017, **56**, 378–394.
- 46 M. A. Dunstan, R. A. Mole and C. Boskovic, *Eur. J. Inorg. Chem.*, 2019, 1090–1105.
- 47 N. F. Chilton, D. Collison, E. J. L. McInnes, R. E. P. Winpenny and A. Soncini, *Nat. Commun.*, 2013, **4**, 2551.
- 48 J. J. Baldoví, S. Cardona-Serra, J. M. Clemente-Juan, E. Coronado, A. Gaita-Ariño and A. Palii, *J. Comput. Chem.*, 2013, **34**, 1961–1967. DOI: 10.1039/C9SC01743G
- 49 L. Ungur and L. F. Chibotaru, *Chem.: Eur. J.*, 2017, **23**, 3708–3718.
- 50 G. Cosquer, F. Pointillart, J. Jung, B. Le Guennic, S. Golhen, O. Cador, Y. Guyot, A. Brenier, O. Maury and L. Ouahab, *Eur. J. Inorg. Chem.*, 2014, **2014**, 69–82.
- 51 J. Jung, O. Cador, K. Bernot, F. Pointillart, J. Luzon and B. Le Guennic, *Beilstein J. Nanotechnol.*, 2014, **5**, 2267–2274.
- 52 S. K. Singh, T. Gupta, L. Ungur and G. Rajaraman, *Chem.: Eur. J.*, 2015, **21**, 13812–13819.
- 53 D. Aravena, M. Atanasov and F. Neese, *Inorg. Chem.*, 2016, **55**, 4457–4469.
- 54 G. Rajaraman, S. K. Singh, B. Pandey and G. Velmurugan, *Dalton Trans.*, 2017, **46**, 11913–11924.
- 55 M.-E. Boulon, G. Cucinotta, J. Luzon, C. Degl'Innocenti, M. Perfetti, K. Bernot, G. Calvez, A. Caneschi and R. Sessoli, *Angew. Chem., Int. Ed.*, 2013, **52**, 350–354.
- 56 J. Jung, M. Atanasov and F. Neese, *Inorg. Chem.*, 2017, **56**, 8802–8816.
- 57 (a) J. Jung, F. Le Natur, O. Cador, F. Pointillart, G. Calvez, C. Daiguebonne, O. Guillou, T. Guizouarn, B. Le Guennic and K. Bernot, *Chem. Commun.*, 2014, **50**, 13346–13348; (b) D. Aravena and E. Ruiz, *Inorg. Chem.*, 2013, **52**, 13770–13778.
- 58 J. Jung, X. Yi, G. Huang, G. Calvez, C. Daiguebonne, O. Guillou, O. Cador, A. Caneschi, T. Roisnel, B. Le Guennic and K. Bernot, *Dalt. Trans.*, 2015, **44**, 18270–18275.
- 59 P. Zhang, J. Jung, L. Zhang, J. Tang and B. Le Guennic, *Inorg. Chem.*, 2016, **55**, 1905–1911.
- 60 M. Voonci, K. Mason, E. A. Sutorina, A. T. Frawley, S. G. Worswick, I. Kuprov, D. Parker, E. J. L. McInnes and N. F. Chilton, *J. Am. Chem. Soc.*, 2017, **139**, 14166–14172.
- 61 E. A. Sutorina, K. Mason, C. F. G. C. Galdes, I. Kuprov and D. Parker, *Angew. Chem., Int. Ed.*, 2017, **56**, 12215–12218.
- 62 F. Pointillart, K. Bernot, S. Golhen, B. Le Guennic, T. Guizouarn, L. Ouahab and O. Cador, *Angew. Chem., Int. Ed. Engl.*, 2014, 1504–1507.
- 63 S. K. Singh, T. Gupta and G. Rajaraman, *Inorg. Chem.*, 2014, **53**, 10835–10845.
- 64 F. Neese, *Wiley Interdiscip. Rev. Comput. Mol. Sci.*, 2012, **2**, 73–78.
- 65 P. J. Stephens, F. J. Devlin, C. F. Chabalowski and M. J. Frisch, *J. Phys. Chem.*, 1994, **98**, 11623–11627.
- 66 S. Grimme, J. Antony, S. Ehrlich and H. Krieg, *J. Chem. Phys.*, 2010, **132**, 0–19.
- 67 D. a. Pantazis and F. Neese, *J. Chem. Theory Comput.*, 2009, **5**, 2229–2238.
- 68 P. E. Blöchl, *J. Chem. Phys.*, 1995, **103**, 7422–7428.
- 69 C. Adamo and V. Barone, *J. Chem. Phys.*, 1999, **110**, 6158–6170.
- 70 J. Hutter, M. Iannuzzi, F. Schiffmann and J. Vandevondele, *Wiley Interdiscip. Rev. Comput. Mol. Sci.*, 2014, **4**, 15–25.
- 71 S. Goedecker, M. Teter and J. Hutter, *Phys. Rev. B*, 1996, **54**, 1703–1710.
- 72 F. Aquilante, J. Autschbach, R. K. Carlson, L. F. Chibotaru, M. G. Delcey, L. De Vico, I. Fdez. Galván, N. Ferré, L. M. Frutos, L. Gagliardi, M. Garavelli, A. Giussani, C. E. Hoyer, G. Li Manni, H. Lischka, D. Ma, P. Å. Malmqvist, T. Müller, A. Nenov, M. Olivucci, T. B. Pedersen, D. Peng, F. Plasser, B. Pritchard, M. Reiher, I. Rivalta, I. Schapiro, J. Segarra-Martí, M. Stenrup, D. G. Truhlar, L. Ungur, A. Valentini, S. Vancouillie, V. Veryazov, V. P. Vysotskiy, O. Weingart, F.



- Zapata and R. Lindh, *J. Comput. Chem.*, 2016, **37**, 506–541.
- 73 J. Luzon and R. Sessoli, *Dalt. Trans.*, 2012, **41**, 13556–13567.
- 74 V. Veryazov, P. A. Malmqvist and B. O. Roos, *Int. J. Quantum Chem.*, 2011, **111**, 3329–3338.
- 75 B. O. Roos, R. Lindh, P. Åke Malmqvist, V. Veryazov and P. O. Widmark, *J. Phys. Chem. A*, 2004, **108**, 2851–2858.
- 76 V. Veryazov, P.-O. Widmark and B. O. Roos, *Theor. Chem. Accounts Theory, Comput. Model. (Theoretica Chim. Acta)*, 2004, **111**, 345–351.
- 77 B. O. B. O. Roos, R. Lindh, P.-A. Malmqvist, V. Veryazov, P.-O. Widmark, A. C. Borin, B. O. Ross, R. Lindh, P.-A. Malmqvist, V. Veryazov, P.-O. Widmark, A. C. Borin, B. O. B. O. Roos, R. Lindh, P.-A. Malmqvist, V. Veryazov, P.-O. Widmark and A. C. Borin, *J. Phys. Chem. A*, 2008, **112**, 11431–11435.
- 78 L. F. Chibotaru and L. Ungur, *J. Chem. Phys.*, 2012, **137**, 064112.
- 79 L. Gagliardi, R. Lindh and G. Karlstrom, *J. Chem. Phys.*, 2004, **121**, 4494.
- 80 P. Söderhjelm, J. W. Krogh, G. Karlström, U. Ryde and R. Lindh, *J. Comput. Chem.*, 2007, **28**, 1083–1090.
- 81 G. Huang, G. Fernandez-Garcia, I. Badiane, M. Camarra, S. Freslon, O. Guillou, C. Daiguebonne, F. Totti, O. Cadot, T. Guizouarn, B. Le Guennic and K. Bernot, *Chem.: Eur. J.*, 2018, **24**, 6983–6991.
- 82 K. Zhang, V. Montigaud, O. Cadot, G.-P. Li, B. Le Guennic, J.-K. Tang and Y.-Y. Wang, *Inorg. Chem.*, 2018, **57**, 8550–8557.
- 83 L. Zhang, J. Jung, P. Zhang, M. Guo, L. Zhao, J. Tang and B. Le Guennic, *Chem.: Eur. J.*, 2016, **22**, 1392–1398.
- 84 E_{cross} can be estimated by the following relation: $E_{\text{cross}} = (E_{1(\alpha = 75^\circ)} + E_{1(\alpha = 105^\circ)})/2 \sim (E_{1(\alpha = 129^\circ)} + E_{1(\alpha = 150^\circ)})/2 \sim (E_{1(\alpha = 245^\circ)} + E_{1(\alpha = 270^\circ)})/2 \sim (E_{1(\alpha = 310^\circ)} + E_{1(\alpha = 330^\circ)})/2$ (see Fig. 5), where the two α values immediately before and after the avoided crossing points ($\alpha = 90^\circ, 140^\circ, 260^\circ, 320^\circ$) are considered.
- 85 S. Niu, M. L. Tan and T. Ichiye, *J. Chem. Phys.*, 2011, **134**, 134501.

View Article Online
DOI: 10.1039/C9SC01743G





View Article Online
DOI: 10.1039/C9SC01743G

The unexpected covalent contribution in DOTADy-OH₂ bond revealed by *ab-initio* calculations of easy axis of magnetization through simple H₂O rotations.

